Molecular Therapy
Nucleic Acids
Original Article

Alternative splicing dysregulation across tissue and therapeutic approaches in a mouse model of myotonic dystrophy type 1

Sawyer M. Hicks,[1,2] Jesus A. Frias,[1,2] Subodh K. Mishra,[2] Marina Scotti,[4] Derek R. Muscato,[4] M. Carmen Valero,[4] Leanne M. Adams,[4] John D. Cleary,[2] Masayuki Nakamori,[3] Eric Wang,[4] and J. Andrew Berglund[1,2]

[1]Department of Biological Sciences, College of Arts and Sciences, University at Albany, SUNY, Albany, NY 12222, USA; [2]The RNA Institute, College of Arts and Sciences, University at Albany, SUNY, Albany, NY 12222, USA; [3]Department of Neurology, Osaka University Graduate School of Medicine, Osaka 565-0871, Japan; [4]Center for NeuroGenetics and Department of Molecular Genetics & Microbiology, College of Medicine, University of Florida, Gainesville, FL 32603, USA

Myotonic dystrophy type 1 (DM1), the leading cause of adult-onset muscular dystrophy, is caused by a CTG repeat expansion. Expression of the repeat causes widespread alternative splicing (AS) defects and downstream pathogenesis, including significant skeletal muscle impacts. The *HSA*^{LR} mouse model plays a significant role in therapeutic development. This mouse model features a transgene composed of approximately 220 interrupted CTG repeats, which results in skeletal muscle pathology that mirrors DM1. To better understand this model and the growing number of therapeutic approaches developed with it, we performed a meta-analysis of publicly available RNA sequencing data for AS changes across three widely examined skeletal muscles: quadriceps, gastrocnemius, and tibialis anterior. Our analysis demonstrated that transgene expression correlated with the extent of splicing dysregulation across these muscles from gastrocnemius (highest), quadriceps (medium), to tibialis anterior (lowest). We identified 95 splicing events consistently dysregulated across all examined datasets. Comparison of splicing rescue across seven therapeutic approaches showed a range of rescue across the 95 splicing events from the three muscle groups. This analysis contributes to our understanding of the *HSA*^{LR} model and the growing number of therapeutic approaches currently in preclinical development for DM1.

INTRODUCTION

Myotonic dystrophy type 1 (DM1) is an autosomal dominant, multisystemic disease that impacts various body systems, including skeletal and smooth muscles, heart, endocrine system, eyes, and the CNS.[1] It is the most prevalent form of adult-onset muscular dystrophy and presents with clinical symptoms that include myotonia, muscle weakness and wasting, cardiac dysfunction, cataracts, insulin resistance, and cognitive impairment. The genetic basis of DM1 is an expansion of a CTG trinucleotide microsatellite repeat in the 3′ UTR of the dystrophia myotonica protein kinase (*DMPK*) gene.[2–5] The molecular underpinnings of the disease are attributed to a toxic RNA gain-of-function model,[6] in which CUG-expanded (CUG^{exp}) RNAs sequester muscleblind-like (MBNL) splicing factors creating nuclear RNA foci.[7–12] Sequestration of MBNL splicing factors disrupts various cellular processes, including alternative splicing (AS), translation, polyadenylation, microRNA processing, and mRNA localization and stability.[8,13–15] Disruptions of key AS events are linked to DM1 symptoms such as myotonia, insulin resistance, and cardiac defects.[16–18]

The use of mouse models to study DM1 has provided critical insights into disease pathology and therapeutic development.[19–27] For example, *Mbnl1* knockout mice closely mimic DM1 symptoms supporting the critical role for *MBNL1* in DM1 pathology.[28] While various mouse models have been used,[29] the *HSA*^{LR} model has played an extensive role in studying DM1.[19,28,30–50,51–73] The *HSA*^{LR} mouse model, expressing ∼220 CUG repeats in the 3′ UTR of the *ACTA1* mRNA, replicates several DM1 features, including central nuclei and ring fibers, variability in fiber size without muscle fiber necrosis, and myotonia. This model replicates the RNA-centric disease pathology driving DM1, without *DMPK* flanking sequences, and has helped cement the central role of the expression of the repeat expansion in disease pathogenesis. Given the use of the mouse model across different studies, there are several RNA sequencing (RNA-seq) studies from muscle tissues from the *HSA*^{LR} mouse,[28,69] especially in studying the response to therapeutic treatments.[31,47,52,59,66]

In this study, we collected publicly available *HSA*^{LR} RNA-seq data along with internal data from our group to analyze *HSA* transgene expression, AS dysregulation, and the impact of seven different therapies tested in the *HSA*^{LR} model. We uncovered previously unreported tissue-specific differences across skeletal muscle groups in *HSA* transgene expression, which directly correlated to AS dysregulation. We also found that the severity of global and shared AS

Received 16 June 2024; accepted 10 September 2024;
https://doi.org/10.1016/j.omtn.2024.102338.

Correspondence: J. Andrew Berglund, Department of Biological Sciences and RNA Institute, College of Arts and Sciences, University at Albany, SUNY, Albany, NY 12222, USA.
E-mail: aberglund@albany.edu

Table 1. Datasets within the meta-analysis

First author	Reference	Method	Read length	Average read depth, million	Tissue
Angelbello	PRJNA525438	rRNA depletion	150	50	Tibialis anterior
Hicks	PRJNA1103789	rRNA depletion	100	115	gastrocnemius, quadriceps, tibialis anterior
Jenquin	PRJNA555349	rRNA depletion	75	80	quadriceps
Klein	PRJNA531100	poly(A) selection	150	80	gastrocnemius, quadriceps
Mishra	PRJNA891268	rRNA depletion	100	110	gastrocnemius
Reddy	PRJNA486539	rRNA depletion	75	65	quadriceps
Solovyeva	E-MTAB-10842	poly(A) selection	75	71	gastrocnemius
Tanner	PRJNA625451	poly(A) selection	125	59	quadriceps

dysregulation across datasets was greater in tissues with higher levels of CUG^{exp} RNA expression, further supporting the RNA gain-of-function model. We identified a set of 95 splicing events consistently dysregulated across all examined datasets. Our comparative analysis of therapeutic responses revealed that several therapeutic approaches rescued a significant portion of dysregulated AS events. Our findings represent a reference for the DM1 research community for understanding and comparing therapeutics studied in the HSA^{LR} model.

RESULTS

RNA-seq data from the HSA^{LR} mouse model

Multiple studies have used muscle tissues harvested from the HSA^{LR} mouse model to generate RNA-seq data and report on transcriptomic effects.[28,31,47,52,59,66,69] In this paper, we set out to understand whether there are differences in AS across these RNA-seq datasets or tissue types and how those differences may change with tissue type and/or expression of CUG^{exp} RNA. To accomplish our goal, we gathered publicly available RNA-seq data (Table 1) and performed detailed transcriptomic analysis. We gathered paired-end RNA-seq data from the published literature[28,31,47,52,59,66,69] from the NCBI Sequence Read Archive (SRA) and the European Molecular Biology Laboratory-European Bioinformatics Institute (EMBNL-EBI) European Nucleotide Archive (ENA), excluding single-end[74] and microarray data.[75] We identified seven existing datasets from our search that examined various muscle groups: gastrocnemius (two studies), quadriceps (three studies), tibialis anterior (TA; one study), and gastrocnemius and quadriceps (one study). We were unable to identify a dataset or study that performed paired-end RNA-seq analysis across all three muscle groups. Given the lack of datasets across the three muscle groups, we generated an additional eighth RNA-seq dataset containing wild-type (WT) and HSA^{LR} samples in triplicate from each tissue source (gastrocnemius, quadriceps, and TA) (Table 1). In total for this study, we utilized eight datasets, encompassing 11 data samples from across three different tissues (four from gastrocnemius, five from quadriceps, and two from TA).

In addition to the variation in muscle groups, the read length, read depth, and preparation methods used to generate the eight selected datasets varied considerably. Of the eight datasets, five were depleted for rRNA, while three were enriched for poly(A) RNA. Given that read length and read depth affects the quantity and quality of detected AS events, we also examined these factors across the datasets. The eight datasets had variable read depths (50–110 million) and read length (75–150 nt), all of which are generally sufficient for AS analysis.[76–78] To account for differences in RNA selection methods, read length, and sequencing depth, our analysis compared WT and HSA^{LR} or HSA^{LR} and treated-HSA^{LR} using a minimum exon and exon junction coverage of 10 reads and two parameters to define dysregulated AS, based on previous literature.[47] Given the mixed reporting across each dataset, we were unable to control for either age or sex across the RNA-seq datasets (Table S1). One dataset[66] did report only HSA^{LR} and HSA^{LR}-treated data but not WT. For analysis of this dataset, we assigned a pseudo-WT sample group from another study[47] that matched the RNA enrichment step, sequencing length, and tissue type. The datasets for our analysis, while variable, provided sufficient quantity and quality of data to enable our meta-analysis.

ACTA1 transgene expression is variable across HSA^{LR} muscle type and is greatest in gastrocnemius

Expression of CUG^{exp} RNA drives MBNL sequestration, resulting in AS dysregulation in DM1.[6–10] In the HSA^{LR} mouse model, the HSA transgene, which contains an interrupted 220 CTG repeat, drives the expression of CUG^{exp} RNA. To estimate the expression of CUG^{exp} RNA across the eight datasets, we generated a custom genome assembly, in which the coding sequence of human *ACTA1* (Gene ID: 58) was inserted into GRCm38/mm39, to which all RNA-seq datasets were aligned. DESeq2-normalized counts of *ACTA1* from each dataset were normalized to *Gtf2b* mRNA as previously described.[47] We found that across the eight datasets, representing 11 samples, *HSA* transgene expression showed a gradient of expression across muscle tissue type from greatest in gastrocnemius, then quadriceps, and lowest expression in TA (Figure 1A). To compare transgene expression differences across tissue types, HSA^{LR} samples were grouped by tissue type and compared using a two-way ANOVA (Figure 1B). This grouped analysis confirmed the individual analysis with a statistically significant difference across the three tissues (two-way ANOVA comparing tissue groups; $p < 0.0001$). To better understand the effects of CUG^{exp} expression on endogenous expression among WT and HSA^{LR} animal models, we examined the expression of the mouse *Acta1*, *Mbnl1*, *Mbnl2*, and *Dmpk* genes (Figure S1). While expression of these mouse genes

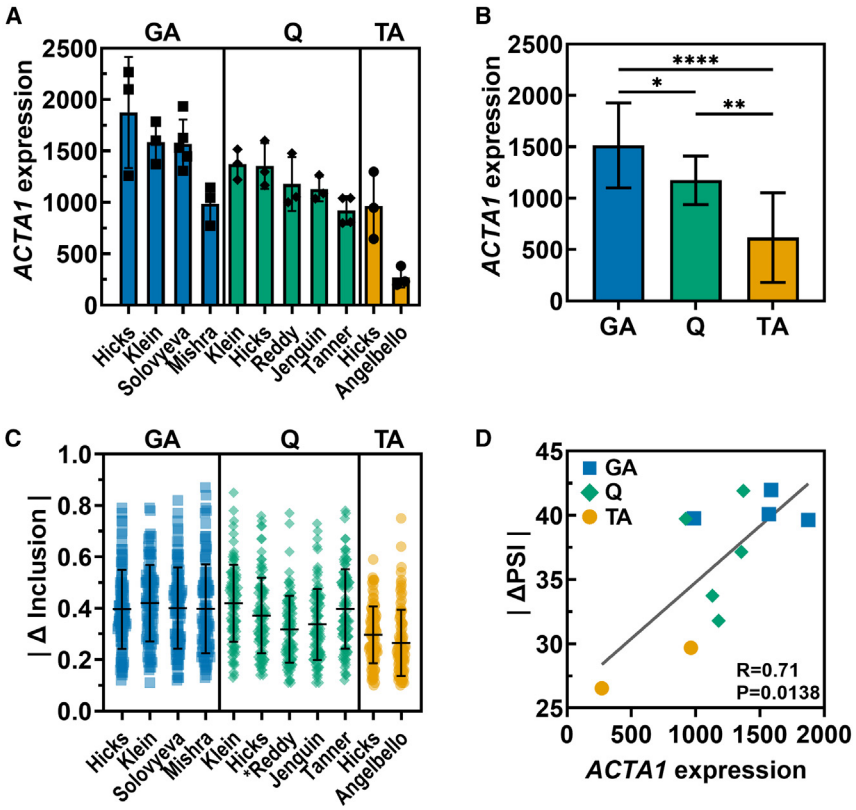

Figure 1. Tissue-specific differences in transgene expression and AS dysregulation in the *HSA*^{LR} mouse model

(A) *ACTA1* transgene expression in gastrocnemius (GA, blue, squares), quadriceps (Q, green, diamonds), and TA (orange, circles) tissues from *HSA*^{LR} mice from each RNA-seq dataset. Data normalized to *Gtf2b* mRNA. Bars represent mean ± SD of biological replicates. (B) *ACTA1* transgene expression grouped by tissue type and statistically compared. *$p < 0.05$; **$p < 0.01$; ****$p < 0.0001$. (C) Absolute inclusion level difference (|Δ Inclusion|) of 95 common and dysregulated (FDR ≤0.05; |Δ Inclusion| ≥ 0.1) AS events among all datasets. (D) Positive correlation of |Δ Inclusion| to *ACTA1* expression normalized to *Gtf2b* (Pearson $r = 0.7127$; $p = 0.0138$).

varied considerably across samples, we did not observe a significant trend among these endogenous genes.

Alternative splicing dysregulation across tissue type and datasets

Dysregulation of AS is a signature molecular hallmark of DM1 and results in a "spliceopathy" that has far-reaching consequences. We next sought to understand the nature and extent of dysregulated AS events within each dataset. To identify dysregulated AS events, *HSA*^{LR} mice were compared to WT mice for each respective study (Table S2). If a dataset published only *HSA*^{LR} RNA-seq and not WT, then a WT group was assigned, and the comparison was denoted with one asterisk in Figures 1C, 2A–2F, and 3A–3D. AS events were considered dysregulated if the false discovery rate (FDR) was ≤0.05 and the absolute exon inclusion level difference (|Δ Inclusion|) was ≥0.1 (Table S3). As anticipated, among each tissue type, skipped exon (SE) events were predominantly dysregulated in each dataset, representing >50% of all events (Figure S2). Retained intron (RI) or mutually exclusive exons (MXEs) were the second most common, followed by alternative 5′ splice sites (A5SS), and then by alternative 3′ splice sites (A3SS) for all datasets.

To better understand how splicing events are shared across different datasets and tissues, we next investigated the number of individual shared events. Events were defined by a unique assigned identifier containing the coordinates of the upstream and downstream start and stop sites for the regulated exon, the upstream exon, and the downstream exon. This stringent approach was utilized to keep the context of the regulated exons intact. Using this unique identifier approach to match events across datasets, we identified the number of shared events that were dysregulated between *HSA*^{LR} and WT mice among two or more datasets of a single tissue type (Figure S3). As anticipated, the number of shared events depended on the number of available datasets for each tissue, with quadriceps (five datasets) having the greatest number of shared events. Across datasets from all tissue types, we identified 95 AS events as significantly dysregulated (Figure S4). Of those 95 shared events, gastrocnemius had the highest level of dysregulation, with a mean |Δ Inclusion| of 0.41 ± 0.15, followed by quadriceps (0.37 ± 0.15), and then TA (0.29 ± 0.12) (Figure 1C). This observation strongly correlated with *ACTA1* expression level differences previously observed (Pearson correlation r(11) = 0.7127; p (two-tailed) = 0.0138) (Figure 1D). To highlight the importance of tissue-specific dysregulation and correlation to CUG^{exp} RNA, we selected 6 AS events (*Atp2a1* exon 22, *Clasp1* exon 20, *Neb* exon 149, *Clcn1* exon 7a, *Nfix* exon 7, and *Mbnl1* exon 5) routinely studied in the DM field for their clinical significance and proposed as splicing biomarkers in animal models and patients. Our analysis of these six AS events (Figures 2A–2F) demonstrates that these events follow the same pattern of tissue-specific dysregulation (gastrocnemius > quadriceps > TA). We also asked whether there were differences in correlation between average positive inclusion-level dysregulation or average negative inclusion-level dysregulation between WT and *HSA*^{LR} groups among the common events. We found that average positive inclusion level dysregulation correlated with muscle type that trended slightly greater than the average negative inclusion-level dysregulation (inclusion: Pearson $r = 0.7239$, $p = 0.0118$; exclusion: Pearson $r = -0.6919$, $p = 0.0183$) (Figure S5). However, comparing these correlations using Hittner, May, and Silver's modification,[79] there was no significant difference between the two overlapping correlations ($z = 0.5504$, $p = 0.5820$). While we observed individual

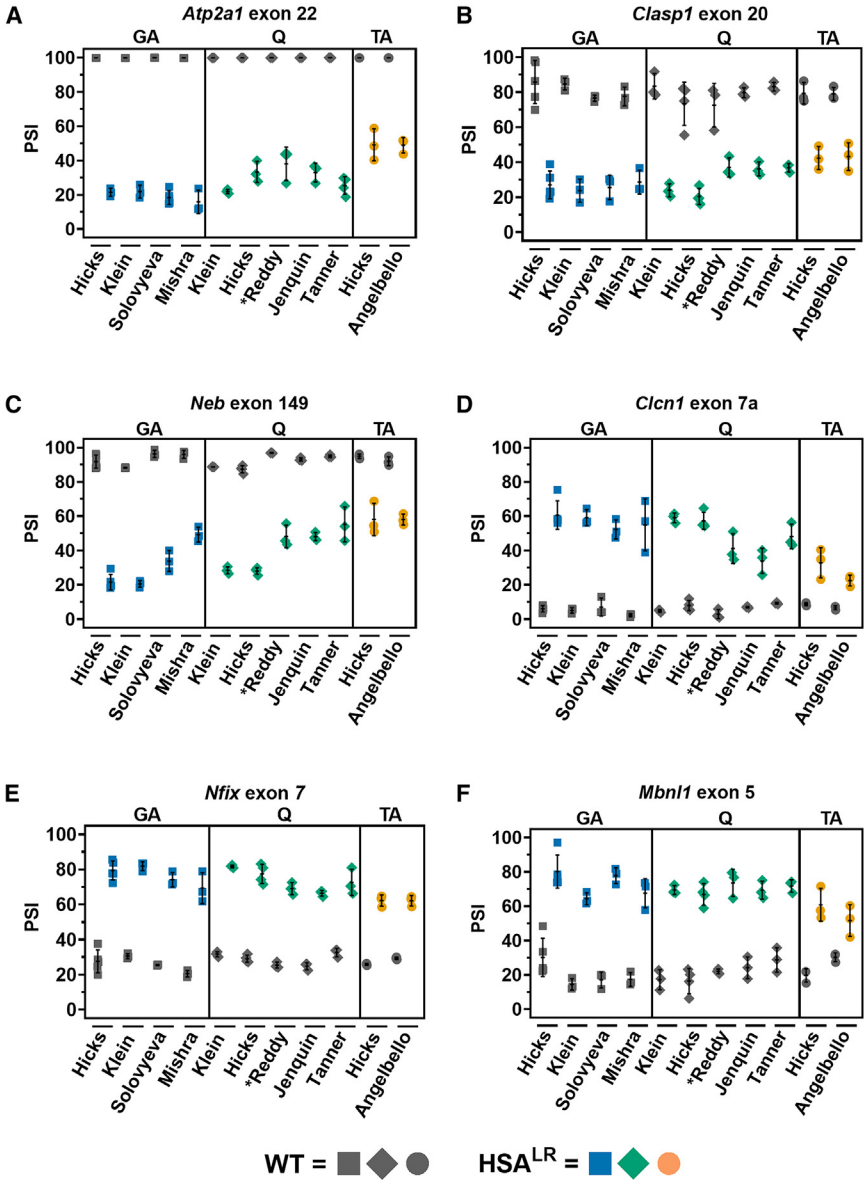

Figure 2. Tissue-specific differences in AS for key events in DM1 and the *HSA*^{LR} mouse model

(A) *Atp2a1* exon 22, (B) *Clasp1* exon 20, (C) *Neb* exon 149, (D) *Clcn1* exon 7a, (E) *Nfix* exon 7, and *Mbnl1* exon 5 (F) mis-splicing events display tissue-specific differences in PSI. WT samples are colored in gray; untreated *HSA*^{LR} mice are colored and shaped by tissue type where gastrocnemius (GA) are blue squares, quadriceps (Q) are green diamonds, and TA are orange circles. Black whiskers depict mean ± SD for sample replicates.

differences between each dataset and across skeletal muscle types, all datasets demonstrate significant spliceopathy, which further confirms the utility of this animal model for therapeutic studies and identifies dysregulation differences by tissue type.

Therapeutic treatment of *HSA*^{LR} mice

The eight datasets in our study represent five publications that cover seven different therapeutic approaches, including small molecules, a natural product, and an antisense oligonucleotide (ASO). For each study, while RNA-seq was utilized to examine AS, the therapeutic approach, time of treatment, and delivery method varied considerably (Table 2). Overall, the number of dysregulated events across the samples ranged from 1,629 (Mishra, gastrocnemius) to 648 events (Angelbello, TA) (Table 3). To determine the therapeutic effect on these dysregulated AS events, percent rescue (see Equation 1) was calculated as previously described.[47] For each dysregulated AS event, the type of rescue was categorized based on percent rescue: rescued (10%–100%), over-rescued (>110%), and mis-rescue (<−10%). The latter category represents exon inclusion levels in treated *HSA*^{LR} mice that shift splicing further from WT levels as compared to untreated *HSA*^{LR}.

For the 10 samples representing the seven different treatments, we calculated the number of rescued, over-rescued, and mis-rescued events and percentage of each category relative to total dysregulated AS events (Table 3). Most treatments rescued >60% of the dysregulated events identified within each study, except for 6-week enzymatically modified isoquercitrin (EMIQ) (49.7%). Furthermore, four of the treatments rescued >70%, including Pip6a-phosphorodiamidate morpholino oligonucleotide (Pip6a-PMO), pafuramidine (PaF) (15 mg/mL), combination of PaF (10 mg/mL) and erythromycin (Em) (600 mg/mL), and cugamycin. Mis-rescued event number varied with treatment, ranging from 3.1% (cugamycin, TA) to 16.6% 6-week EMIQ. Pip6aPMO, the only treatment for which datasets from multiple tissues (gastrocnemius and quadriceps) were available performed similarly across tissues, with a high average rescue of 75.9% and a low average mis-rescue of 4.25%.

Off-target events are a significant concern for any therapeutic treatment, even for precisely targeted gene therapies. To better understand potential off-target events from treatment, we categorized an event as off-target if the event met the following conditions: a $|\Delta \text{ Inclusion}| \geq 0.2$ between treated and non-treated *HSA*^{LR} mice, the event was not considered dysregulated between WT and *HSA*^{LR} (FDR >0.05 and $|\Delta \text{ Inclusion}| < 0.1$), and the event had a small SD measured within WT and *HSA*^{LR} groups (≤ 0.1). From this analysis, across the 10 samples from the treatment datasets, <1% of all events following treatment were classified as off-target (Table 4), and not a single off-target event

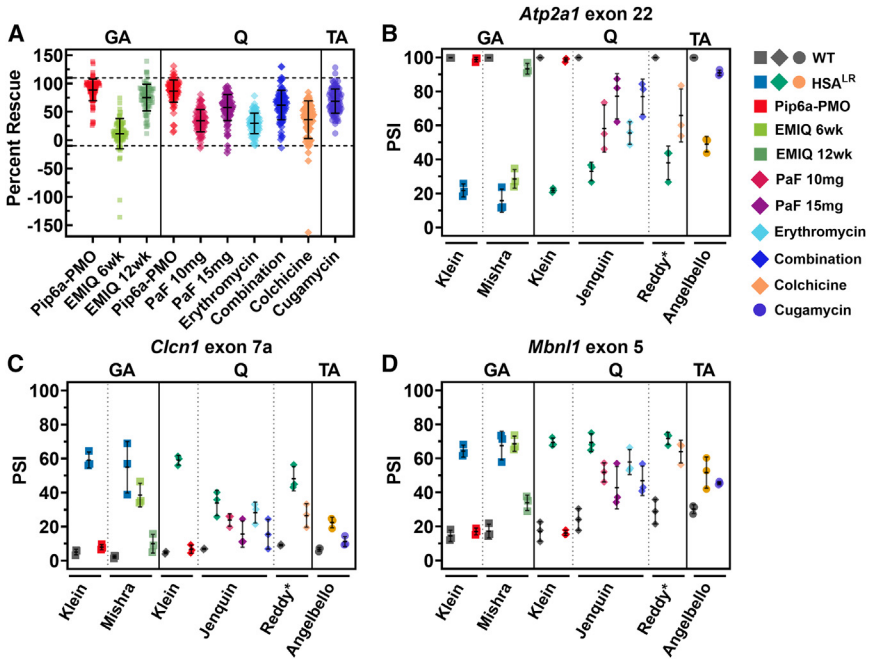

Figure 3. Treatment effects of published therapeutics in the *HSA*^{LR} model

(A) Distribution of percent rescue scores among the dysregulated AS events common to all datasets. PSI values for WT, *HSA*^{LR}, and treated-*HSA*^{LR} groups are shown for the individual events (B) *Atp2a1* exon 22, (C) *Clcn1* exon 7a, and (D) *Mbnl1* exon 5. Black whiskers depict mean ± SD for sample replicates.

was common to all therapeutic approaches. We are cognizant that the overall variability in splicing when comparing WT, *HSA*^{LR}, and treated *HSA*^{LR} groups complicates the assessment of off-target changes.

Given the variability in AS events across tissues and treatments, we next assessed how the 95 shared dysregulated SE events (Table 5) responded across each treatment. By focusing on only shared events, we were able to more clearly understand how each therapeutic approach affected dysregulated SE events in a side-by-side comparison. The distribution of percent rescue scores for the 95 common events were plotted (Figure 3A), and for the events found to be rescued by each therapeutic, the scores were binned and summarized (Table 5). We found that the distribution of shared events rescued by Pip6a-PMO centered around 90% rescue, whereas PaF, Em, combination treatment of Paf and Em, and cugamycin centered at or <70% rescue. Individual effects by treatment were also reported by percent spliced in (PSI), which is the exon inclusion level multiplied by 100, in a heatmap format (Figure S6).

From the binned analysis (Table 5), we observed that Pip6a-PMO treatment in both gastrocnemius or quadriceps rescued more events toward the upper end of rescue (80%–100%) compared to other treatments, with gastrocnemius having a more robust rescue effect on dysregulated events. Analysis of splicing events associated with DM1, such as *Atp2a1* exon 22, *Clcn1* exon7a, and *Mbnl1* exon 5 (Figures 3B–3D) showed the same trend as the overall analysis.

From the binned analysis, we observed several phenomena. For EMIQ at 6 weeks, there was rescue of 52 of 95 events, mostly centered on the 10%–20% rescue bin; whereas after 12 weeks of EMIQ treatment, 84 of 95 events showed rescue, with 66 AS events surpassing >60% rescue. This increase in splicing rescue matches the buildup of molecular and phenotypic responses observed by Mishra and colleagues.[59] Aligning with this buildup effect for EMIQ that we observed at 6 weeks of treatment, 12 of the 95 events responded negatively (more dysregulated than untreated *HSA*^{LR}); interestingly, those events were rescued after 12 weeks of treatment. For example, *App* exon 15 at EMIQ 6 weeks had a −15% rescue and at 12 weeks, it had a 119% rescue (Figure S7C). A similar increased effect on splicing rescue in the shared events was observed with increasing PaF treatment (10–15 mg/kg) from the Jenquin et al. study.[47] Rescue of *Atp2a1* exon 22 (Figure 3B) and *Clasp1* exon 20 (Figure S7A), among other events, demonstrated a dose-related response. Additionally, in this study, while both Em and PaF had modest effects (∼80 events rescued), the combination treatment of PaF and Em had additive effects on splicing rescue. Combination treatment increased both the

Table 2. Therapeutic summary table organized by author, tissue, therapeutic and dosage, approach, time, and delivery method

First author	Therapeutic and dose	Time	Delivery	Approach
Angelbello	cugamycin (10 mg/kg)	every other day for 1 week (4 total)	IP injection	cleaves CUG^{exp} RNA
Klein	peptide-conjugated oligos (Pip6a-PMO) (12.5 mg/kg)	1 injection every 2 weeks (3 total)	IM injection	anneals CUG^{exp} RNA
Jenquin	PaF (10 mg/kg, 15 mg/kg), Em (600 mg/kg)	daily for 2 weeks (14 total)	oral delivery in corn oil	PaF binds CUG^{exp} RNA; Em upregulates *MBNL* expression
Mishra	EMIQ (1.5 g/L, 15 g/L)	daily for 12 weeks (persistent)	oral via drinking water	reduce CUG^{exp} RNA expression
Reddy	colch (0.4 mg/kg)	daily for 14 days (14 total)	IP injection	destabilize microtubule formation reducing CUG^{exp} RNA expression

Colch, colchicine; IM, intramuscular; IP, intraperitoneal; Pip6a-PMO, Pip6A-phosphorodiamidate morpholino oligonucleotide

Table 3. Rescue, mis-rescue, and over-rescue total treatment effect by therapeutic

Therapeutic	Reference	Total events	Rescue (%)	Over-rescue (%)	Mis-rescue (%)
Gastrocnemius					
Pip6a-PMO	Klein PRJNA531100	1,394	1,042 (74.7)	171 (12.3)	54 (3.8)
EMIQ 6 weeks	Mishra PRJNA891268	1,629	810 (49.7)	133 (8.2)	270 (16.6)
EMIQ 12 weeks			1,064 (65.3)	125 (7.7)	130 (8.0)
Quadriceps					
Pip6a-PMO	Klein PRJNA531100	1,358	1,047 (77.1)	144 (10.6)	64 (4.7)
PaF 10 mg/kg	Jenquin PRJNA555349	1,124	762 (67.8)	46 (4.1)	128 (11.4)
PaF 15 mg/kg			829 (73.8)	68 (6.0)	88 (7.8)
Em 600 mg/kg			780 (69.4)	35 (3.1)	117 (10.4)
PaF and EM combination[a]			824 (73.3)	71 (6.3)	73 (6.5)
Colchicine	Reddy PRJNA486539	1,096	675 (61.6)	41 (3.7)	78 (7.1)
TA					
Cugamycin	Angelbello PRJNA525438	648	502 (77.5)	71 (11.0)	20 (3.1)

[a]PaF 10 mg/kg + Em 600 mg/kg.

Table 4. Off-target effects of each therapeutic

Therapeutic	Total unchanged events	Off-target
Gastrocnemius		
Pip6a-PMO	39,238	274
EMIQ 6 weeks	27,313	115
EMIQ 12 weeks		132
Quadriceps		
Pip6a-PMO	38,050	220
PaF 10 mg/kg	30,839	240
PaF 15 mg/kg		289
Em 600 mg/kg		283
Combination (PaF 10 mg/kg + Em 600 mg/kg)		289
Colchicine	31,101	235
TA		
Cugamycin	26,389	335

Unchanged events are those that are not dysregulated between WT and HSALR mice (FDR >0.05, |Δ Inclusion| < 0.1). Off-target events are those that are not dysregulated between WT and HSALR mice and that deviated ≤0.1, and |Δ Inclusion| of HSALR and HSALR treated ≥0.2.

total number of rescued shared events and the distribution of extent of rescue, with most shared AS events showing rescue between 50% and 80%. It is interesting to note that cugamycin positively affected all 95 shared dysregulated events, like Pip6a-PMO treatments, but the overall degree of rescue was not as robust, with most events rescuing between 50% and 70% compared to >80% for Pip6A-PMO. Of all the treatments, colchicine rescued the fewest number of shared events (48 of 95), but of those events rescued, most were >50% rescue. These data indicate a diverse response at the level of splicing rescue to various therapeutic approaches, with all treatments providing robust rescue of shared AS events and minimal off-target effects.

Recently, Tanner and colleagues published a panel of 36 splicing events for targeted RNA-seq in DM1 mouse models, 35 of which are dysregulated in mouse models of DM1.[28] We examined our eight datasets for these events and identified 34 of the 36 splicing events (Figure S8). We should note that when comparing methods, we used the same alignment software, HISAT2, but with different version numbers (Hicks version 2.2.1; Tanner version 2.1.0). The reference genomes also differed (Tanner GRCm38/mm10; Hicks GRCm39/mm39). Tanner et al. used an isoform-specific counting approach to calculate PSI. We used rMATS-turbo-calculated inclusion levels. Despite these pipeline differences, compared to our criteria for dysregulation (FDR ≤ 0.05 and $|\Delta \text{ Inclusion}| \geq 0.1$), most events matched their designation as dysregulated events, with TA having fewer events dysregulated (Figure S9). We checked how these events responded to treatment effect (Figure S10) and observed a comparable range of effects compared to the 95 commonly dysregulated SE events identified in this study (Figure 3A). All events from the targeted RNA-seq panel exhibited a treatment response. The responses to therapeutic treatment were similar between the Tanner et al. panel of 35 events and our shared 95 events, supporting the utilization of shared splicing events as a splicing biomarker in DM1.

DISCUSSION

DM1 is a complex muscular dystrophy affecting various tissue systems and resulting in symptoms that range from myotonia to cognitive impairment. This highly diverse set of symptoms stem from the expression of toxic CUG^{exp} and a resulting RNA gain-of-function mechanism that leads to the dysregulation of AS and downstream pathology. Here, we performed a meta-analysis of RNA-seq data from the HSA^{LR} mouse model, investigating AS dysregulation and therapeutic responses across different studies and between different skeletal muscle types. Our analysis demonstrated that CUG^{exp} transgene expression correlated with the level of splicing dysregulation across gastrocnemius (highest), quadriceps (medium), and TA (lowest). We identified many AS events that were dysregulated across the datasets, as well as events that responded to treatment effect by each respective therapeutic. Off-target splicing analysis identified no common off-target effect across the therapeutic treatments. We also identified a set of 95 shared events consistently dysregulated across all HSA^{LR} datasets and muscle groups and used those events as a basis for side-by-side comparison across therapeutics. Comparison of splicing rescue for these events across the seven therapeutics showed unique distribution patterns that highlighted the overall effect of each therapeutic. Additionally, we identified individual splicing events that were easier to rescue, like *Atp2a1* exon 22, *Clcn1* exon 7a, and *Mbnl1*

Table 5. Therapeutic effect on commonly dysregulated AS events

Therapeutic	Total	>10%	>20%	>30%	>40%	>50%	>60%	>70%	>80%	>90%	>100%
Gastrocnemius											
Pip6a-PMO	95	–	2	2	–	4	5	9	18	35	20
EMIQ 6 weeks	52	24	14	7	4	1	1	1	–	–	–
EMIQ 12 weeks	84	1	4	2	5	6	12	15	15	16	8
Quadriceps											
Pip6a-PMO	95	2	2	–	1	2	4	16	23	27	18
PaF 10 mg/kg	84	10	15	27	12	10	6	3	1	–	–
PaF 15 mg/kg	90	2	3	5	10	18	29	8	11	4	–
Em 600 mg/kg	80	13	21	17	14	13	1	1	–	–	–
Combination (PaF 10 mg/kg + Em 600 mg/kg)	90	1	3	8	9	14	19	20	6	3	7
Colchicine	64	8	6	4	1	3	5	9	6	6	16
TA											
Cugamycin	95	1	1	5	9	22	13	14	12	12	6

exon 5, and splicing events that were difficult to rescue, like *App* exon 15 and *Ttn* exon 348 (Figure S7). Some dysregulated splicing events were found to be over-rescued after therapeutic treatment, meaning an event surpassed WT levels by >9 PSI and responded strongly to treatment. This is a good indication of the effect of a therapeutic and provides a metric that may indicate a particular molecular mechanism. Readers should also note that the WT baseline used in these studies are FVB/NJ multipurpose inbred mice. The distribution of PSI for this population can vary across colonies and time, which we observed in these data. Sampling more WT-classified mouse strains would result in a greater distribution of PSI levels for each individual event. Therefore, rescue and under-rescue classifications would shift based on the WT mouse strain compared to and we do not take this into account in these comparisons. This analysis contributes to our understanding of the HSA^{LR} model and the growing number of therapeutic approaches in development for DM1.

Our analysis of therapeutic responses in HSA^{LR} mice recapitulated promising outcomes for several therapeutics, including Pip6a-PMO, EMIQ, combination treatment of PaF and Em, and cugamycin, which improved the mis-splicing of a significant number of shared AS events. Notably, Pip6a-PMO, 12-week EMIQ, and cugamycin showed no mis-rescue for the 95 shared dysregulated AS events. We also identified AS events common to all datasets that were more easily rescued and less easily rescued. Each therapeutic and the dosage for the studies had a range of effects on AS events, which provides insights into the responsiveness to treatment of an individual AS event. For example, while Pip6a-PMO largely rescued AS events to within 90% rescue, *Arfip1* exon 4 rescued to 26% in gastrocnemius and to 16% in quadriceps. Interestingly, 12-week EMIQ, combination treatment, and cugamycin had robust effects on this event, rescuing to 86%, 76%, and 92%, respectively. While individual splicing events can be closely connected with symptoms in DM1 patients, such as CLCN1 and myotonia, there are many dysregulated events not specifically tied to symptoms. As such, it is difficult to predict or assess the efficacy of a therapeutic treatment based upon a single mis-splicing event, such as *Arfip* exon 4. Rather, our analysis and others (Tanner and colleagues[28]) speaks to the power of assessing a panel of mis-splicing events along with off-target events to determine therapeutic efficacy.

In conclusion, our study offers insights into AS dysregulation and therapeutic responses in the DM1 HSA^{LR} mouse model. Through our investigation, we reported tissue-specific differences in transgene expression and identified a subset of shared dysregulated AS events present across three skeletal muscle tissues. These findings have implications for the DM1 research community and can inform the efforts of academic and industry research groups in therapeutic development. By collating these datasets, investigating AS dysregulation, and highlighting effective therapeutic strategies, our study contributes to the collective understanding of DM1 pathology and brings us closer to the development of targeted treatments for this debilitating disease.

MATERIALS AND METHODS

Mouse husbandry

Animal care procedures for the following mice were performed in accordance with the University of Florida Animal Care and Use Committee. Six mice, three FVB/NJ (WT) and three HSA^{LR} were used for the analysis. WT mice were 15 weeks and 6 days old and HSA^{LR} mice were 16 weeks old on the day of sacrifice. Details on oversight for animals associated with other data can be found in their respective publications.

RNA extraction from muscle tissue

Mouse tissues from TA, quadriceps, and gastrocnemius were handled identically. Tissues were lysed and homogenized with 800 μL TRIzol reagent (Thermo Fisher Scientific, 15596018) in 2-mL tubes pre-filled with 1.5-mm high impact zirconium beads (Benchmark Scientific, D1032-15). Tubes were agitated at 5,000 × *g* for 1 min using a

Bead Ruptor 12 (OMNI International, 19-050A). Then, they were placed on ice for 1 min, for a total of five repetitions for complete tissue lysis. RNA was then extracted following the Directzol RNA Miniprep Plus kit (Zymo Research, R2070). RNA concentration was measured using a Nanodrop One spectrophotometer (Thermo Fisher Scientific, ND-ONE-W).

Library preparation

RNA integrity was assessed by measuring the RNA integrity number using capillary electrophoresis (Agilent, M5310AA) paired with the RNA kit (Agilent, DNF-471-0500). A total of 500 ng RNA was used as input for library preparation. rRNA was depleted from samples (NEB, E7405), and libraries were prepared for paired-end Illumina sequencing (NEB, E7760L) with the following adjustments to the manufacturer's protocol: 1:40 adaptor dilution, universal and indexing primers at 1 μM final concentration, and 10 cycles for PCR enrichment of adaptor ligated DNA. Library quality was assessed via capillary gel electrophoresis (Agilent, M5310AA) paired with the High Sensitivity Next Generation Sequencing Fragment Kit (Agilent, DNF-474-0500). Library concentrations were determined via qPCR (Bio-Rad, 1855484) using a Library Quant Kit for Illumina (NEB, E7630L) following the manufacturer's protocol.

RNA-seq

Sequencing libraries were pooled to 2 nM and diluted to a final loading concentration of 650 pM with a PhiX (Illumina, FC-110-3002) spike in of 5%. Sequencing was performed on the Illumina NextSeq 2000 platform (Illumina, 20038897) using the onboard denature and dilute protocol, paired with P3 reagents for 200 cycles (Illumina, 20040560). Sequencing output was demultiplexed and converted to FASTQ format via Basespace BCL Convert (version 2.3.0).

RNA-seq data analysis

RNA-seq FASTQ files were collected from the NCBI SRA or the EMBNL-EBIENA) databases using SRA Toolkit (version 3.0.5) or FTP Client, respectively. FASTQ file quality and total number of reads were assessed using FASTQC (version 0.11.9) and datasets with an average read depth >35 million paired-end reads were accepted for this study. Sequencing reads were trimmed, and low-quality reads were filtered using FASTP (version 0.23.4)[80] under default settings. FASTQ files were aligned to the GRCm39/mm39 reference genome, which was modified to include the human *ACTA1* coding sequence, using HISAT2 (version 2.2.1).[81] The resulting SAM file output was reformatted to BAM format using SAMtools (version 1.17).[82]

Gene expression analysis

To measure differential gene expression, RNA-seq alignments were assembled into potential transcripts using StringTie (version 2.2.0),[81] and read count information was extracted using prepDE.py3. Each dataset was analyzed independently with R (version 4.3.1) using DESeq2 (version 1.40.1).[83] DESeq2-normalized counts were used to measure gene expression from each dataset. To compare across datasets, gene expression values were normalized to *Gtf2b*.

Alternative splicing analysis

Each dataset was analyzed independently using rMATS-turbo (version 4.2.0),[84] with BAM files as input and with the optional flags "–allow-clipping" and "–variable-read-length." If authors did not publish a WT group of mice in their study, then a pseudo-WT was assigned from a different publication. To match AS events across datasets, a unique ID was generated for each event using all positional coordinates provided in the rMATS JCEC output files for all JCEC files (SE, A5SS, A3SS, MXE, RI). The unique ID contained the Ensembl ID and gene symbol preceding the event coordinates, followed by the event type (e.g., *ENSMUSG00000027763_Mbnl1_chr3_+_60436176_60437225_60380462_60380594_60503014_60503185_SE*). This approach maintained the regulated exon(s) of interest and the context in which the exons are regulated. AS events were considered to be dysregulated according to the FDR (≤ 0.05) and absolute value of the inclusion level difference ($|\Delta \text{ Inclusion}| \geq 0.1$) when comparing HSA^{LR} mice to WT mice. When combining comparisons within datasets (i.e., WT vs. HSA^{LR} and HSA^{LR} vs. HSA^{LR} treated), tables were matched by the unique IDs. This method was also applied when joining AS data across datasets. To determine the effect of a therapeutic treatment on a given dysregulated AS event, Equation 1 was used to find %Rescue. $HSA^{LR}{}_{PSI}$ indicates the PSI of untreated HSA^{LR} mice, $Drug_{PSI}$ indicates the PSI of treated HSA^{LR} mice, and WT_{PSI} indicates the PSI of WT mice. The %Rescue allows the interpretation of treatment, where a return to WT inclusion levels in treated HSA^{LR} mice results in a value of 100% and the treatment effect is categorized as "rescue." An effect resulting in >110% Rescue is categorized as "over-rescue" and <−10% Rescue is categorized as "mis-rescue."

$$\%\ \text{Rescue} = \left[\frac{HSA^{LR}_{PSI} - \text{Drug}_{PSI}}{HSA^{LR}_{PSI} - \text{WT}_{PSI}}\right] \times 100 \qquad \text{(Equation 1)}$$

Statistical analysis

AS statistical tests comparing WT and HSA^{LR} or HSA^{LR} and treated HSA^{LR} were performed concurrently with rMATS-turbo with default settings. Two-way ANOVA statistical tests were performed in GraphPad Prism, testing the null hypothesis of no difference among the group means. Hypergeometric testing for Venn diagrams was performed within Flaski,[85] assessing the significance of observing the number of common AS events among tissue types from the sample population of total events.

DATA AND CODE AVAILABILITY

RNA-seq data from each study is publicly available on the NCBI SRA and the EMBNL-EBI ENA. A complete list of studies used is available in the supplemental information. RNA-seq libraries prepared for this study are available on SRA under PRJNA1103789. The codes for data processing can be found on GitHub (https://github.com/SawyerHicks/*HSA*-LR-Alternative-Splicing-Analysis).

ACKNOWLEDGMENTS

We thank the Berglund and Wang labs for helpful advice on the research and manuscript. This work was supported by an RNA Fellowship from NIH T32 GM132066 (to S.M.H.), MDF Fellowships (to J.A.F. and S.K.M.), USAMRAA CDMRP HT9425-24-1-0191 PRMRP (to J.A.B. and J.D.C.), NIH R01 NS135254 (to J.A.B. and J.D.C.), Muscular Dystrophy Association award no. 1192211 (to J.A.B.), and R01 NS120485 (to J.A.B. and

J.D.C.). This work was also supported by a Chan-Zuckerberg Initiative Ben Barres Early Career Acceleration Award to E.W. The content of this article is solely the responsibility of the authors and does not necessarily represent the official views of the NIH or other funding agencies.

AUTHOR CONTRIBUTIONS

J.A.B. and J.D.C. conceived and designed the study and contributed to critical revisions of the manuscript. S.M.H. performed the research, bioinformatic analysis, and drafted the manuscript. J.A.F. and S.K.M. extracted RNA from mouse tissue and prepared the RNA-seq libraries. M.S. and E.W. from the University of Florida and M.N. from the Osaka University Graduate School of Medicine provided mouse tissues for sequencing.

DECLARATION OF INTERESTS

J.A.B. serves on the Scientific Advisory Committee for the Myotonic Dystrophy Foundation, has consulted or currently consults for Entrada Therapeutics, Juvena Therapeutics, Kate Therapeutics, D.E. Shaw Research, Dyne Therapeutics, Syros Pharmaceuticals, and Wayfinder Biosciences, and has received research funding from Agios Pharmaceuticals, Biomarin Pharmaceuticals, PepGen, Syros Pharmaceuticals, and Vertex Pharmaceuticals. E.T.W. is a co-founder and consultant to Kate Therapeutics. J.A.B. has received licensing royalties from the University of Florida. J.A.B. and J.D.C. are co-founders and have a financial interest in Repeat RNA Therapeutics Inc. J.D.C. is a part-time employee of the Center for NeuroGenetics at the University of Florida.

SUPPLEMENTAL INFORMATION

Supplemental information can be found online at https://doi.org/10.1016/j.omtn.2024.102338.

REFERENCES

1. Ozimski, L.L., Sabater-Arcis, M., Bargiela, A., and Artero, R. (2021). The hallmarks of myotonic dystrophy type 1 muscle dysfunction. Biol. Rev. Camb. Philos. Soc. *96*, 716–730. https://doi.org/10.1111/brv.12674.

2. Brook, J.D., McCurrach, M.E., Harley, H.G., Buckler, A.J., Church, D., Aburatani, H., Hunter, K., Stanton, V.P., Thirion, J.P., Hudson, T., et al. (1992). Molecular basis of myotonic dystrophy: expansion of a trinucleotide (CTG) repeat at the 3' end of a transcript encoding a protein kinase family member. Cell *68*, 799–808. https://doi.org/10.1016/0092-8674(92)90154-5.

3. Buxton, J., Shelbourne, P., Davies, J., Jones, C., Van Tongeren, T., Aslanidis, C., de Jong, P., Jansen, G., Anvret, M., Riley, B., et al. (1992). Detection of an unstable fragment of DNA specific to individuals with myotonic dystrophy. Nature *355*, 547–548. https://doi.org/10.1038/355547a0.

4. Mahadevan, M., Tsilfidis, C., Sabourin, L., Shutler, G., Amemiya, C., Jansen, G., Neville, C., Narang, M., Barceló, J., O'Hoy, K., et al. (1992). Myotonic dystrophy mutation: an unstable CTG repeat in the 3' untranslated region of the gene. Science *255*, 1253–1255. https://doi.org/10.1126/science.1546325.

5. Fu, Y.H., Pizzuti, A., Fenwick, R.G., Jr., King, J., Rajnarayan, S., Dunne, P.W., Dubel, J., Nasser, G.A., Ashizawa, T., de Jong, P., et al. (1992). An unstable triplet repeat in a gene related to myotonic muscular dystrophy. Science *255*, 1256–1258. https://doi.org/10.1126/science.1546326.

6. Thornton, C.A. (2014). Myotonic dystrophy. Neurol. Clin. *32*, 705–719. viii. https://doi.org/10.1016/j.ncl.2014.04.011.

7. Mohan, A., Goodwin, M., and Swanson, M.S. (2014). RNA-protein interactions in unstable microsatellite diseases. Brain Res. *1584*, 3–14. https://doi.org/10.1016/j.brainres.2014.03.039.

8. Goodwin, M., and Swanson, M.S. (2014). RNA-binding protein misregulation in microsatellite expansion disorders. Adv. Exp. Med. Biol. *825*, 353–388. https://doi.org/10.1007/978-1-4939-1221-6_10.

9. Jiang, H., Mankodi, A., Swanson, M.S., Moxley, R.T., and Thornton, C.A. (2004). Myotonic dystrophy type 1 is associated with nuclear foci of mutant RNA, sequestration of muscleblind proteins and deregulated alternative splicing in neurons. Hum. Mol. Genet. *13*, 3079–3088. https://doi.org/10.1093/hmg/ddh327.

10. Mankodi, A., Lin, X., Blaxall, B.C., Swanson, M.S., and Thornton, C.A. (2005). Nuclear RNA foci in the heart in myotonic dystrophy. Circ. Res. *97*, 1152–1155. https://doi.org/10.1161/01.RES.0000193598.89753.e3.

11. Lin, X., Miller, J.W., Mankodi, A., Kanadia, R.N., Yuan, Y., Moxley, R.T., Swanson, M.S., and Thornton, C.A. (2006). Failure of MBNL1-dependent post-natal splicing transitions in myotonic dystrophy. Hum. Mol. Genet. *15*, 2087–2097. https://doi.org/10.1093/hmg/ddl132.

12. Fardaei, M., Rogers, M.T., Thorpe, H.M., Larkin, K., Hamshere, M.G., Harper, P.S., and Brook, J.D. (2002). Three proteins, MBNL, MBLL and MBXL, co-localize in vivo with nuclear foci of expanded-repeat transcripts in DM1 and DM2 cells. Hum. Mol. Genet. *11*, 805–814. https://doi.org/10.1093/hmg/11.7.805.

13. Masuda, A., Andersen, H.S., Doktor, T.K., Okamoto, T., Ito, M., Andresen, B.S., and Ohno, K. (2012). CUGBP1 and MBNL1 preferentially bind to 3' UTRs and facilitate mRNA decay. Sci. Rep. *2*, 209. https://doi.org/10.1038/srep00209.

14. Wang, E.T., Taliaferro, J.M., Lee, J.A., Sudhakaran, I.P., Rossoll, W., Gross, C., Moss, K.R., and Bassell, G.J. (2016). Dysregulation of mRNA Localization and Translation in Genetic Disease. J. Neurosci. *36*, 11418–11426. https://doi.org/10.1523/JNEUROSCI.2352-16.2016.

15. Batra, R., Charizanis, K., Manchanda, M., Mohan, A., Li, M., Finn, D.J., Goodwin, M., Zhang, C., Sobczak, K., Thornton, C.A., and Swanson, M.S. (2014). Loss of MBNL leads to disruption of developmentally regulated alternative polyadenylation in RNA-mediated disease. Mol. Cell *56*, 311–322. https://doi.org/10.1016/j.molcel.2014.08.027.

16. Dixon, D.M., Choi, J., El-Ghazali, A., Park, S.Y., Roos, K.P., Jordan, M.C., Fishbein, M.C., Comai, L., and Reddy, S. (2015). Loss of muscleblind-like 1 results in cardiac pathology and persistence of embryonic splice isoforms. Sci. Rep. *5*, 9042. https://doi.org/10.1038/srep09042.

17. Mankodi, A., Takahashi, M.P., Jiang, H., Beck, C.L., Bowers, W.J., Moxley, R.T., Cannon, S.C., and Thornton, C.A. (2002). Expanded CUG repeats trigger aberrant splicing of ClC-1 chloride channel pre-mRNA and hyperexcitability of skeletal muscle in myotonic dystrophy. Mol. Cell *10*, 35–44. https://doi.org/10.1016/s1097-2765(02)00563-4.

18. Savkur, R.S., Philips, A.V., and Cooper, T.A. (2001). Aberrant regulation of insulin receptor alternative splicing is associated with insulin resistance in myotonic dystrophy. Nat. Genet. *29*, 40–47. https://doi.org/10.1038/ng704.

19. Mankodi, A., Logigian, E., Callahan, L., McClain, C., White, R., Henderson, D., Krym, M., and Thornton, C.A. (2000). Myotonic dystrophy in transgenic mice expressing an expanded CUG repeat. Science *289*, 1769–1773. https://doi.org/10.1126/science.289.5485.1769.

20. Seznec, H., Lia-Baldini, A.S., Duros, C., Fouquet, C., Lacroix, C., Hofmann-Radvanyi, H., Junien, C., and Gourdon, G. (2000). Transgenic mice carrying large human genomic sequences with expanded CTG repeat mimic closely the DM CTG repeat intergenerational and somatic instability. Hum. Mol. Genet. *9*, 1185–1194. https://doi.org/10.1093/hmg/9.8.1185.

21. Guiraud-Dogan, C., Huguet, A., Gomes-Pereira, M., Brisson, E., Bassez, G., Junien, C., and Gourdon, G. (2007). DM1 CTG expansions affect insulin receptor isoforms expression in various tissues of transgenic mice. Biochim. Biophys. Acta *1772*, 1183–1191. https://doi.org/10.1016/j.bbadis.2007.08.004.

22. Vignaud, A., Ferry, A., Huguet, A., Baraibar, M., Trollet, C., Hyzewicz, J., Butler-Browne, G., Puymirat, J., Gourdon, G., and Furling, D. (2010). Progressive skeletal muscle weakness in transgenic mice expressing CTG expansions is associated with the activation of the ubiquitin-proteasome pathway. Neuromuscul. Disord. *20*, 319–325. https://doi.org/10.1016/j.nmd.2010.03.006.

23. Jansen, G., Groenen, P.J., Bächner, D., Jap, P.H., Coerwinkel, M., Oerlemans, F., van den Broek, W., Gohlsch, B., Pette, D., Plomp, J.J., et al. (1996). Abnormal myotonic dystrophy protein kinase levels produce only mild myopathy in mice. Nat. Genet. *13*, 316–324. https://doi.org/10.1038/ng0796-316.

24. Reddy, S., Smith, D.B., Rich, M.M., Leferovich, J.M., Reilly, P., Davis, B.M., Tran, K., Rayburn, H., Bronson, R., Cros, D., et al. (1996). Mice lacking the myotonic dystrophy protein kinase develop a late onset progressive myopathy. Nat. Genet. *13*, 325–335. https://doi.org/10.1038/ng0796-325.

25. Sarkar, P.S., Appukuttan, B., Han, J., Ito, Y., Ai, C., Tsai, W., Chai, Y., Stout, J.T., and Reddy, S. (2000). Heterozygous loss of Six5 in mice is sufficient to cause ocular cataracts. Nat. Genet. *25*, 110–114. https://doi.org/10.1038/75500.

26. O'Cochlain, D.F., Perez-Terzic, C., Reyes, S., Kane, G.C., Behfar, A., Hodgson, D.M., Strommen, J.A., Liu, X.K., van den Broek, W., Wansink, D.G., et al. (2004).

Transgenic overexpression of human DMPK accumulates into hypertrophic cardiomyopathy, myotonic myopathy and hypotension traits of myotonic dystrophy. Hum. Mol. Genet. *13*, 2505–2518. https://doi.org/10.1093/hmg/ddh266.

27. Wang, G.S., Kearney, D.L., De Biasi, M., Taffet, G., and Cooper, T.A. (2007). Elevation of RNA-binding protein CUGBP1 is an early event in an inducible heart-specific mouse model of myotonic dystrophy. J. Clin. Invest. *117*, 2802–2811. https://doi.org/10.1172/JCI32308.

28. Tanner, M.K., Tang, Z., and Thornton, C.A. (2021). Targeted splice sequencing reveals RNA toxicity and therapeutic response in myotonic dystrophy. Nucleic Acids Res. *49*, 2240–2254. https://doi.org/10.1093/nar/gkab022.

29. Gomes-Pereira, M., Cooper, T.A., and Gourdon, G. (2011). Myotonic dystrophy mouse models: towards rational therapy development. Trends Mol. Med. *17*, 506–517. https://doi.org/10.1016/j.molmed.2011.05.004.

30. Alvarez-Abril, M.C., Garcia-Alcover, I., Colonques-Bellmunt, J., Garijo, R., Perez-Alonso, M., Artero, R., and Lopez-Castel, A. (2023). Natural Compound Boldine Lessens Myotonic Dystrophy Type 1 Phenotypes in DM1 Drosophila Models, Patient-Derived Cell Lines, and HSA(LR) Mice. Int. J. Mol. Sci. *24*, 9820. https://doi.org/10.3390/ijms24129820.

31. Angelbello, A.J., Rzuczek, S.G., McKee, K.K., Chen, J.L., Olafson, H., Cameron, M.D., Moss, W.N., Wang, E.T., and Disney, M.D. (2019). Precise small-molecule cleavage of an r(CUG) repeat expansion in a myotonic dystrophy mouse model. Proc. Natl. Acad. Sci. USA *116*, 7799–7804. https://doi.org/10.1073/pnas.1901484116.

32. Banks, G.B., Combs, A.C., Chamberlain, J.R., and Chamberlain, J.S. (2008). Molecular and cellular adaptations to chronic myotendinous strain injury in mdx mice expressing a truncated dystrophin. Hum. Mol. Genet. *17*, 3975–3986. https://doi.org/10.1093/hmg/ddn301.

33. Bargiela, A., Sabater-Arcis, M., Espinosa-Espinosa, J., Zulaica, M., Lopez de Munain, A., and Artero, R. (2019). Increased Muscleblind levels by chloroquine treatment improve myotonic dystrophy type 1 phenotypes in in vitro and in vivo models. Proc. Natl. Acad. Sci. USA *116*, 25203–25213. https://doi.org/10.1073/pnas.1820297116.

34. Bargiela, A., Ten-Esteve, A., Martí-Bonmatí, L., Sevilla, T., Perez Alonso, M., and Artero, R. (2023). Quantitative magnetic resonance imaging assessment of muscle composition in myotonic dystrophy mice. Sci. Rep. *13*, 503. https://doi.org/10.1038/s41598-023-27661-w.

35. Bisset, D.R., Stepniak-Konieczna, E.A., Zavaljevski, M., Wei, J., Carter, G.T., Weiss, M.D., and Chamberlain, J.R. (2015). Therapeutic impact of systemic AAV-mediated RNA interference in a mouse model of myotonic dystrophy. Hum. Mol. Genet. *24*, 4971–4983. https://doi.org/10.1093/hmg/ddv219.

36. Brockhoff, M., Rion, N., Chojnowska, K., Wiktorowicz, T., Eickhorst, C., Erne, B., Frank, S., Angelini, C., Furling, D., Rüegg, M.A., et al. (2017). Targeting deregulated AMPK/mTORC1 pathways improves muscle function in myotonic dystrophy type I. J. Clin. Invest. *127*, 549–563. https://doi.org/10.1172/JCI89616.

37. Cerro-Herreros, E., González-Martínez, I., Moreno, N., Espinosa-Espinosa, J., Fernández-Costa, J.M., Colom-Rodrigo, A., Overby, S.J., Seoane-Miraz, D., Poyatos-García, J., Vilchez, J.J., et al. (2021). Preclinical characterization of antagomiR-218 as a potential treatment for myotonic dystrophy. Mol. Ther. Nucleic Acids *26*, 174–191. https://doi.org/10.1016/j.omtn.2021.07.017.

38. Cerro-Herreros, E., González-Martínez, I., Moreno-Cervera, N., Overby, S., Pérez-Alonso, M., Llamusí, B., and Artero, R. (2020). Therapeutic Potential of AntagomiR-23b for Treating Myotonic Dystrophy. Mol. Ther. Nucleic Acids *21*, 837–849. https://doi.org/10.1016/j.omtn.2020.07.021.

39. Cerro-Herreros, E., Sabater-Arcis, M., Fernandez-Costa, J.M., Moreno, N., Perez-Alonso, M., Llamusi, B., and Artero, R. (2018). miR-23b and miR-218 silencing increase Muscleblind-like expression and alleviate myotonic dystrophy phenotypes in mammalian models. Nat. Commun. *9*, 2482. https://doi.org/10.1038/s41467-018-04892-4.

40. Chen, G., Masuda, A., Konishi, H., Ohkawara, B., Ito, M., Kinoshita, M., Kiyama, H., Matsuura, T., and Ohno, K. (2016). Phenylbutazone induces expression of MBNL1 and suppresses formation of MBNL1-CUG RNA foci in a mouse model of myotonic dystrophy. Sci. Rep. *6*, 25317. https://doi.org/10.1038/srep25317.

41. Choi, J., Personius, K.E., DiFranco, M., Dansithong, W., Yu, C., Srivastava, S., Dixon, D.M., Bhatt, D.B., Comai, L., Vergara, J.L., and Reddy, S. (2015). Muscleblind-Like 1 and Muscleblind-Like 3 Depletion Synergistically Enhances Myotonia by Altering Clc-1 RNA Translation. EBioMedicine *2*, 1034–1047. https://doi.org/10.1016/j.ebiom.2015.07.028.

42. Crawford Parks, T.E., Marcellus, K.A., Péladeau, C., Jasmin, B.J., and Ravel-Chapuis, A. (2020). Overexpression of Staufen1 in DM1 mouse skeletal muscle exacerbates dystrophic and atrophic features. Hum. Mol. Genet. *29*, 2185–2199. https://doi.org/10.1093/hmg/ddaa111.

43. DiFranco, M., Yu, C., Quiñonez, M., and Vergara, J.L. (2013). Age-dependent chloride channel expression in skeletal muscle fibres of normal and HSA(LR) myotonic mice. J. Physiol. *591*, 1347–1371. https://doi.org/10.1113/jphysiol.2012.246546.

44. Gonzalez-Martinez, I., Cerro-Herreros, E., Moreno, N., Garcia-Rey, A., Espinosa-Espinosa, J., Carrascosa-Saez, M., Piqueras-Losilla, D., Arzumanov, A., Seoane-Miraz, D., Jad, Y., et al. (2023). Peptide-conjugated antimiRs improve myotonic dystrophy type 1 phenotypes by promoting endogenous MBNL1 expression. Mol. Ther. Nucleic Acids *34*, 102024. https://doi.org/10.1016/j.omtn.2023.09.001.

45. Gudde, A.E.E.G., González-Barriga, A., van den Broek, W.J.A.A., Wieringa, B., and Wansink, D.G. (2016). A low absolute number of expanded transcripts is involved in myotonic dystrophy type 1 manifestation in muscle. Hum. Mol. Genet. *25*, 1648–1662. https://doi.org/10.1093/hmg/ddw042.

46. Huang, K., Wang, D.D., Hu, W.B., Zeng, W.Q., Xu, X., Li, Q.X., Bi, F.F., Yang, H., and Qiu, J. (2022). Calcitriol increases MBNL1 expression and alleviates myotonic dystrophy phenotypes in HSA(LR) mouse models. J. Transl. Med. *20*, 588. https://doi.org/10.1186/s12967-022-03806-9.

47. Jenquin, J.R., Yang, H., Huigens, R.W., 3rd, Nakamori, M., and Berglund, J.A. (2019). Combination Treatment of Erythromycin and Furamidine Provides Additive and Synergistic Rescue of Mis-Splicing in Myotonic Dystrophy Type 1 Models. ACS Pharmacol. Transl. Sci. *2*, 247–263. https://doi.org/10.1021/acsptsci.9b00020.

48. Jones, K., Wei, C., Iakova, P., Bugiardini, E., Schneider-Gold, C., Meola, G., Woodgett, J., Killian, J., Timchenko, N.A., and Timchenko, L.T. (2012). GSK3beta mediates muscle pathology in myotonic dystrophy. J. Clin. Invest. *122*, 4461–4472. https://doi.org/10.1172/JCI64081.

49. Kanadia, R.N., Shin, J., Yuan, Y., Beattie, S.G., Wheeler, T.M., Thornton, C.A., and Swanson, M.S. (2006). Reversal of RNA missplicing and myotonia after muscleblind overexpression in a mouse poly(CUG) model for myotonic dystrophy. Proc. Natl. Acad. Sci. USA *103*, 11748–11753. https://doi.org/10.1073/pnas.0604970103.

50. Ketley, A., Wojciechowska, M., Ghidelli-Disse, S., Bamborough, P., Ghosh, T.K., Morato, M.L., Sedehizadeh, S., Malik, N.A., Tang, Z., Powalowska, P., et al. (2020). CDK12 inhibition reduces abnormalities in cells from patients with myotonic dystrophy and in a mouse model. Sci. Transl. Med. *12*, eaaz2415. https://doi.org/10.1126/scitranslmed.aaz2415.

51. Kimura, T., Nakamori, M., Lueck, J.D., Pouliquin, P., Aoike, F., Fujimura, H., Dirksen, R.T., Takahashi, M.P., Dulhunty, A.F., and Sakoda, S. (2005). Altered mRNA splicing of the skeletal muscle ryanodine receptor and sarcoplasmic/endoplasmic reticulum Ca2+-ATPase in myotonic dystrophy type 1. Hum. Mol. Genet. *14*, 2189–2200. https://doi.org/10.1093/hmg/ddi223.

52. Klein, A.F., Varela, M.A., Arandel, L., Holland, A., Naouar, N., Arzumanov, A., Seoane, D., Revillod, L., Bassez, G., Ferry, A., et al. (2019). Peptide-conjugated oligonucleotides evoke long-lasting myotonic dystrophy correction in patient-derived cells and mice. J. Clin. Invest. *129*, 4739–4744. https://doi.org/10.1172/JCI128205.

53. Koebis, M., Kiyatake, T., Yamaura, H., Nagano, K., Higashihara, M., Sonoo, M., Hayashi, Y., Negishi, Y., Endo-Takahashi, Y., Yanagihara, D., et al. (2013). Ultrasound-enhanced delivery of morpholino with Bubble liposomes ameliorates the myotonia of myotonic dystrophy model mice. Sci. Rep. *3*, 2242. https://doi.org/10.1038/srep02242.

54. Leger, A.J., Mosquea, L.M., Clayton, N.P., Wu, I.H., Weeden, T., Nelson, C.A., Phillips, L., Roberts, E., Piepenhagen, P.A., Cheng, S.H., and Wentworth, B.M. (2013). Systemic delivery of a Peptide-linked morpholino oligonucleotide neutralizes mutant RNA toxicity in a mouse model of myotonic dystrophy. Nucleic Acid Ther. *23*, 109–117. https://doi.org/10.1089/nat.2012.0404.

55. Li, M., Zhuang, Y., Batra, R., Thomas, J.D., Li, M., Nutter, C.A., Scotti, M.M., Carter, H.A., Wang, Z.J., Huang, X.S., et al. (2020). HNRNPA1-induced spliceopathy in a transgenic mouse model of myotonic dystrophy. Proc. Natl. Acad. Sci. USA *117*, 5472–5477. https://doi.org/10.1073/pnas.1907297117.

56. Lueck, J.D., Mankodi, A., Swanson, M.S., Thornton, C.A., and Dirksen, R.T. (2007). Muscle chloride channel dysfunction in two mouse models of myotonic dystrophy. J. Gen. Physiol. *129*, 79–94. https://doi.org/10.1085/jgp.200609635.

57. Lutz, M., Levanti, M., Karns, R., Gourdon, G., Lindquist, D., Timchenko, N.A., and Timchenko, L. (2023). Therapeutic Targeting of the GSK3beta-CUGBP1 Pathway in Myotonic Dystrophy. Int. J. Mol. Sci. *24*, 10650. https://doi.org/10.3390/ijms241310650.

58. Manta, A., Stouth, D.W., Xhuti, D., Chi, L., Rebalka, I.A., Kalmar, J.M., Hawke, T.J., and Ljubicic, V. (2019). Chronic exercise mitigates disease mechanisms and improves muscle function in myotonic dystrophy type 1 mice. J. Physiol. *597*, 1361–1381. https://doi.org/10.1113/JP277123.

59. Mishra, S.K., Hicks, S.M., Frias, J.A., Vangaveti, S., Nakamori, M., Cleary, J.D., Reddy, K., and Berglund, J.A. (2023). Quercetin selectively reduces expanded repeat RNA levels in models of myotonic dystrophy. Preprint at bioRxiv. https://doi.org/10.1101/2023.02.02.526846.

60. Moyer, M., Berger, D.S., Ladd, A.N., and Van Lunteren, E. (2011). Differential susceptibility of muscles to myotonia and force impairment in a mouse model of myotonic dystrophy. Muscle Nerve *43*, 818–827. https://doi.org/10.1002/mus.21988.

61. Neault, N., Ravel-Chapuis, A., Baird, S.D., Lunde, J.A., Poirier, M., Staykov, E., Plaza-Diaz, J., Medina, G., Abadía-Molina, F., Jasmin, B.J., and MacKenzie, A.E. (2023). Vorinostat Improves Myotonic Dystrophy Type 1 Splicing Abnormalities in DM1 Muscle Cell Lines and Skeletal Muscle from a DM1 Mouse Model. Int. J. Mol. Sci. *24*, 3794. https://doi.org/10.3390/ijms24043794.

62. Negishi, Y., Endo-Takahashi, Y., and Ishiura, S. (2018). Exon Skipping by Ultrasound-Enhanced Delivery of Morpholino with Bubble Liposomes for Myotonic Dystrophy Model Mice. Methods Mol. Biol. *1828*, 481–487. https://doi.org/10.1007/978-1-4939-8651-4_30.

63. Ohsawa, N., Koebis, M., Mitsuhashi, H., Nishino, I., and Ishiura, S. (2015). ABLIM1 splicing is abnormal in skeletal muscle of patients with DM1 and regulated by MBNL, CELF and PTBP1. Gene Cell. *20*, 121–134. https://doi.org/10.1111/gtc.12201.

64. Overby, S.J., Cerro-Herreros, E., Espinosa-Espinosa, J., González-Martínez, I., Moreno, N., Fernández-Costa, J.M., Balaguer-Trias, J., Ramón-Azcón, J., Pérez-Alonso, M., Møller, T., et al. (2023). BlockmiR AONs as Site-Specific Therapeutic MBNL Modulation in Myotonic Dystrophy 2D and 3D Muscle Cells and HSA(LR) Mice. Pharmaceutics *15*, 1118. https://doi.org/10.3390/pharmaceutics15041118.

65. Ravel-Chapuis, A., Al-Rewashdy, A., Bélanger, G., and Jasmin, B.J. (2018). Pharmacological and physiological activation of AMPK improves the spliceopathy in DM1 mouse muscles. Hum. Mol. Genet. *27*, 3361–3376. https://doi.org/10.1093/hmg/ddy245.

66. Reddy, K., Jenquin, J.R., McConnell, O.L., Cleary, J.D., Richardson, J.I., Pinto, B.S., Haerle, M.C., Delgado, E., Planco, L., Nakamori, M., et al. (2019). A CTG repeat-selective chemical screen identifies microtubule inhibitors as selective modulators of toxic CUG RNA levels. Proc. Natl. Acad. Sci. USA *116*, 20991–21000. https://doi.org/10.1073/pnas.1901893116.

67. Sabater-Arcis, M., Moreno, N., Sevilla, T., Perez Alonso, M., Bargiela, A., and Artero, R. (2024). Msi2 enhances muscle dysfunction in a myotonic dystrophy type 1 mouse model. Biomed. J. *47*, 100667. https://doi.org/10.1016/j.bj.2023.100667.

68. Sharp, L., Cox, D.C., and Cooper, T.A. (2019). Endurance exercise leads to beneficial molecular and physiological effects in a mouse model of myotonic dystrophy type 1. Muscle Nerve *60*, 779–789. https://doi.org/10.1002/mus.26709.

69. Solovyeva, E.M., Utzinger, S., Vissières, A., Mitchelmore, J., Ahrné, E., Hermes, E., Poetsch, T., Ronco, M., Bidinosti, M., Merkl, C., et al. (2022). Integrative proteogenomics for differential expression and splicing variation in a DM1 mouse model. Preprint at bioRxiv. https://doi.org/10.1101/2021.05.15.443842.

70. Stoodley, J., Miraz, D.S., Jad, Y., Fischer, M., Wood, M.J.A., and Varela, M.A. (2023). Peptide-Conjugated PMOs for the Treatment of Myotonic Dystrophy. Methods Mol. Biol. *2587*, 209–237. https://doi.org/10.1007/978-1-0716-2772-3_13.

71. Wang, M., Weng, W.C., Stock, L., Lindquist, D., Martinez, A., Gourdon, G., Timchenko, N., Snape, M., and Timchenko, L. (2019). Correction of Glycogen Synthase Kinase 3beta in Myotonic Dystrophy 1 Reduces the Mutant RNA and Improves Postnatal Survival of DMSXL Mice. Mol. Cell Biol. *39*, e00155-19. https://doi.org/10.1128/MCB.00155-19.

72. Wei, C., Jones, K., Timchenko, N.A., and Timchenko, L. (2013). GSK3beta is a new therapeutic target for myotonic dystrophy type 1. Rare Dis. *1*, e26555. https://doi.org/10.4161/rdis.26555.

73. Wei, C., Stock, L., Valanejad, L., Zalewski, Z.A., Karns, R., Puymirat, J., Nelson, D., Witte, D., Woodgett, J., Timchenko, N.A., and Timchenko, L. (2018). Correction of GSK3beta at young age prevents muscle pathology in mice with myotonic dystrophy type 1. FASEB J. *32*, 2073–2085. https://doi.org/10.1096/fj.201700700R.

74. Siboni, R.B., Nakamori, M., Wagner, S.D., Struck, A.J., Coonrod, L.A., Harriott, S.A., Cass, D.M., Tanner, M.K., and Berglund, J.A. (2015). Actinomycin D Specifically Reduces Expanded CUG Repeat RNA in Myotonic Dystrophy Models. Cell Rep. *13*, 2386–2394. https://doi.org/10.1016/j.celrep.2015.11.028.

75. Wheeler, T.M., Leger, A.J., Pandey, S.K., MacLeod, A.R., Nakamori, M., Cheng, S.H., Wentworth, B.M., Bennett, C.F., and Thornton, C.A. (2012). Targeting nuclear RNA for in vivo correction of myotonic dystrophy. Nature *488*, 111–115. https://doi.org/10.1038/nature11362.

76. Wang, Y., Xie, Z., Kutschera, E., Adams, J.I., Kadash-Edmondson, K.E., and Xing, Y. (2024). rMATS-turbo: an efficient and flexible computational tool for alternative splicing analysis of large-scale RNA-seq data. Nat. Protoc. *19*, 1083–1104. https://doi.org/10.1038/s41596-023-00944-2.

77. Shen, S., Park, J.W., Huang, J., Dittmar, K.A., Lu, Z.X., Zhou, Q., Carstens, R.P., and Xing, Y. (2012). MATS: a Bayesian framework for flexible detection of differential alternative splicing from RNA-Seq data. Nucleic Acids Res. *40*, e61. https://doi.org/10.1093/nar/gkr1291.

78. Vaquero-Garcia, J., Barrera, A., Gazzara, M.R., González-Vallinas, J., Lahens, N.F., Hogenesch, J.B., Lynch, K.W., and Barash, Y. (2016). A new view of transcriptome complexity and regulation through the lens of local splicing variations. Elife *5*, e11752. https://doi.org/10.7554/eLife.11752.

79. Hittner, J.B., May, K., and Silver, N.C. (2003). A Monte Carlo evaluation of tests for comparing dependent correlations. J. Gen. Psychol. *130*, 149–168. https://doi.org/10.1080/00221300309601282.

80. Chen, S., Zhou, Y., Chen, Y., and Gu, J. (2018). fastp: an ultra-fast all-in-one FASTQ preprocessor. Bioinformatics *34*, i884–i890. https://doi.org/10.1093/bioinformatics/bty560.

81. Pertea, M., Kim, D., Pertea, G.M., Leek, J.T., and Salzberg, S.L. (2016). Transcript-level expression analysis of RNA-seq experiments with HISAT, StringTie and Ballgown. Nat. Protoc. *11*, 1650–1667. https://doi.org/10.1038/nprot.2016.095.

82. Li, H., Handsaker, B., Wysoker, A., Fennell, T., Ruan, J., Homer, N., Marth, G., Abecasis, G., and Durbin, R.; 1000 Genome Project Data Processing Subgroup (2009). The Sequence Alignment/Map format and SAMtools. Bioinformatics *25*, 2078–2079. https://doi.org/10.1093/bioinformatics/btp352.

83. Love, M.I., Huber, W., and Anders, S. (2014). Moderated estimation of fold change and dispersion for RNA-seq data with DESeq2. Genome Biol. *15*, 550. https://doi.org/10.1186/s13059-014-0550-8.

84. Shen, S., Park, J.W., Lu, Z.X., Lin, L., Henry, M.D., Wu, Y.N., Zhou, Q., and Xing, Y. (2014). rMATS: robust and flexible detection of differential alternative splicing from replicate RNA-Seq data. Proc. Natl. Acad. Sci. USA *111*, E5593–E5601. https://doi.org/10.1073/pnas.1419161111.

85. Iqbal, A., Duitama, C., Metge, F., Rosskopp, D., & Boucas, J. (2021). Flaski (2.0.0).